DOI: 10.1021/ma1001194

Macromolecules
ARTICLE

Surface Effects on the Thin Film Morphology of Block Copolymers with Bulk Order−Order Transitions

Karen E. Sohn,[†] Ken Kojio,[‡] Brian C. Berry,[§,#] Alamgir Karim,[§,×] Robert C. Coffin,[∥] Guillermo C. Bazan,[∥] Edward J. Kramer,*[,†,▽] Michael Sprung,[⊥,◆] and Jin Wang[⊥]

[†]*Department of Materials, University of California, Santa Barbara, Santa Barbara, California 93106,* [‡]*Department of Materials Science and Engineering, Nagasaki University, Nagasaki, 852-8521, Japan,* [§]*Polymers Division, National Institute of Standards and Technology, Gaithersburg, Maryland 20899,* [∥]*Department of Chemistry and Biochemistry, University of California, Santa Barbara, Santa Barbara, California 93106, and* [⊥]*Advanced Photon Source, Argonne National Laboratory, Argonne, Illinois 60439.* [#]*Current address: Department of Chemistry, University of Arkansas at Little Rock.* [×]*Current address: College of Polymer Science and Polymer Engineering, University of Akron.* [▽]*Department of Chemical Engineering, University of California, Santa Barbara.* [◆]*Current address: HASYLAB, DESY.*

Received January 17, 2010; Revised Manuscript Received February 21, 2010

ABSTRACT: The morphology of poly(styrene-*b*-ethylene-*r*-butylene) (SEB) and poly(styrene-*b*-ethylene-*r*-butylene-*b*-styrene) (SEBS) thin films annealed both above (165 °C) and below (125 °C) the bulk order−order transition temperatures (OOT) (∼140 °C) was characterized with grazing incidence small-angle X-ray scattering (GISAXS), dynamic secondary ion mass spectrometry (d-SIMS), and atomic force microscopy (AFM). The SEBS thin film morphology is always spherical, regardless of film thickness or annealing temperature, leading us to conclude that the OOT for films up to five layers of spheres is depressed by at least 10 °C relative to the bulk. In contrast, the SEB film morphology at both 125 and 165 °C is always cylindrical, except when the film thickness is less than t_{cyl}, a monolayer of cylinders. For SEB film thicknesses, t, less than t_{cyl} at 165 °C either a partial or full monolayer of spheres forms (thickness t_{sph}) with coexistence of patches of spheres and cylinders when $t_{sph} < t < t_{cyl}$. Thus, we conclude that the OOT for SEB film thickness between t_{cyl} and $5t_{cyl}$ is increased by at least 20 °C over that of the bulk. This complex phase behavior can be understood qualitatively by considering two small contributions to the free energy f per block copolymer chain in the films: (1) an increase in f due to packing frustration and (2) a decrease in f due to the entropy of chain ends near the block copolymer film surfaces. The SEBS has no chain ends near the surface, and we propose that the larger packing frustration of SEBS chains in the square Wigner−Seitz cells of the cylinder monolayer, and the surface half-layers in thicker films, leads to the stabilization of the spherical morphology, which has a smaller packing frustration in the monolayer and surface half-layers. The SEB cylinders and sphere monolayers have the same packing frustration as those of the SEBS, but the contribution of the added entropy of chain ends near the surface is larger for the cylinders than for the spheres, more than offsetting the effect of packing frustration and thus stabilizing the cylindrical morphology at temperatures above the OOT.

Introduction

Thin films of block copolymers have been the focus of much research because of the ability to control the placement of ordered microdomains. Producing films with large areas of defect free order is essential to realize the goal of using block copolymers in memory storage applications. The self-assembly properties of block copolymers allow them to be used as templates for structures smaller than the current limits of photolithography.[1,2] Several different block copolymer morphologies have been studied for this purpose, including spherical domains, lamellar domains oriented perpendicular to the substrate, and cylinders oriented both parallel and perpendicular to the substrate.[3−10] For example, Stoykovich et al. have produced many of the block copolymer structures that are required in integrated circuit geometries using chemically patterned substrates, removing the size constraints imposed by optical lithography.[11]

There has been a great deal of research studying block copolymers with an order−order transition (OOT), both in the bulk melt[12−24] and in solution.[25−27] These studies investigated transitions induced by temperature, shear forces, and electric fields. Sakurai et al. were the first to observe the transition between spheres and cylinders as the temperature is changed.[12] Sota et al. studied the kinetics of the transition from disordered spheres to hexagonal cylinders in a poly(styrene-*b*-isoprene-*b*-styrene) (SIS) triblock copolymer in bulk and found that, depending on the quench temperature, the process will be either one or two steps, with body-centered cubic (BCC) spheres forming before cylinders when the quench temperature is not far below the order−order transition temperature.[22] Koppi et al. determined that the transition from cylinders to spheres occurs epitaxially, with the cylinder axes transformed into the ⟨111⟩ direction of spheres in the BCC lattice,[13] which is in agreement with theoretical predictions by Matsen[18] and with more recent experiments.[16,22] A limited amount of work has studied OOT's in thin films.[28,29] Xu et al. used electric fields to cause poorly ordered spheres of poly(styrene-*b*-methyl methacrylate) diblock copolymer to undergo a change from spheres to hexagonally ordered cylinders oriented perpendicular to the substrate and parallel to the electric field.[28] Very recently, Shin and co-workers published a careful grazing incidence X-ray scattering study of the OOTs in

*To whom correspondence should be addressed. E-mail: edkramer@mrl.ucsb.edu.

 Published on Web 03/10/2010

a poly(styrene-*b*-isoprene) diblock copolymer which underwent thermal transitions from disordered to hexagonal cylinders to gyroid to hexagonally perforated lamellae to lamellae on cooling.[30] The films were rather thick (about 40 lamellar layers), and the OOTs shifted to higher temperatures with the loss of the hexagonal cylinder phase.

Because of surface and interfacial effects, the thickness of the film can cause a different morphology than the equilibrium bulk morphology to have the lowest free energy, resulting in a changing morphology as the film thickness increases. Several studies, both experimental and theoretical, have shown that the film thickness can induce changes in the thin film morphology from the expected bulk morphology.[31−35] Anastasiadis et al. were among the first to study the behavior of symmetric diblock copolymer thin films in comparison with the bulk. This work found that the preferential wetting of one of the two blocks at an interface causes the lamellae to be oriented parallel to the interface. Knoll et al. found that an ABA triblock copolymer with a bulk cylindrical morphology forms a variety of morphologies in thin films depending on thickness. As the film thickness increases, they observed cylinders oriented perpendicular to the surface, followed by parallel cylinders, perforated lamellae, parallel, and then perpendicular cylinders. Dynamic density functional theory (DDFT) calculations produce morphologies that are in agreement with the experimental results.[33,36,37] Similar experimental and theoretical work by Ludwigs et al. found that an ABC triblock copolymer also shows a thickness-dependent morphology that deviates from what is seen in the bulk.[34,35] Non-equilibrium bulk structures including perforated lamellae are also sometimes stabilized at certain film thicknesses.[33,35,36]

This paper focuses on block copolymer systems of poly(styrene-*b*-ethylene-*r*-butylene) (SEB) and poly(styrene-*b*-ethylene-*r*-butylene-*b*-styrene) (SEBS) with compositions close enough to the transition between cylinders and spheres in the phase diagram that the equilibrium morphology will change depending on the annealing temperature.[38] These systems have several advantages over other often-studied block copolymer systems. The ODT is accessible and is sufficiently far above the glass transition temperature to allow for experiments over a range of temperatures. The modulus difference between the blocks provides contrast in atomic force microscopy (AFM) phase images, so that no destructive techniques are required in order to image the surface of the sample. Using films with a gradient in film thickness, the variations in sample preparation can be removed, and the morphology as a function of film thickness can be determined using a small number of samples. AFM will be used to characterize the surface structure, while grazing incidence small-angle X-ray scattering (GISAXS) will be used to characterize the structure throughout the thickness of the film. Dynamic secondary ion mass spectrometry (d-SIMS) will be used to determine the number of microdomain layers at each thickness of the gradient thickness film. In contrast to the experiments reported by Shin et al.,[30] the focus of our experiments reported below is on the effects of film thickness on the structure of these block copolymer films at two temperatures, one above and one below the OOT.

Experimental Section

The polymers used in these experiments were extracted from Kraton 1657, a commercial blend of SEB and SEBS, which has an overall composition of 65 wt % SEBS and 35 wt % SEB. The properties of the blend have been described elsewhere.[14] The blend was separated into the individual components (each ~95% pure) by fractional precipitation using selective solvents.[38]

Silva et al. have characterized the order−order transition (OOT) and order−disorder transition (ODT) temperatures for both the blend and the fractionated SEB and SEBS.[38] Table 1 shows the OOT and ODT for all three polymers. Small-angle X-ray scattering (SAXS) at UCSB measured the OOTs and showed that they are in agreement with those of Silva et al.[38,39]

Table 1. OOT and ODT for the Blend, Diblock, and Triblock As Determined by Silva et al.[38] [a]

polymer	OOT (°C)	ODT (°C)
blend	138 ± 3	196 ± 2
diblock	143 ± 3	192 ± 2
triblock	136 ± 2	199 ± 2

[a] The ODT's were determined by small-angle neutron scattering (SANS), and the OOT's were determined by linear viscoelastic measurements using isochronal plots at a zero heating rate.

The polystyrene blocks of the separated block copolymers were selectively deuterated using a method developed by Willenberg, resulting in a 75% exchange of deuterium atoms for the aromatic protons in the polystyrene block of the SEB and a greater than 95% exchange in the SEBS.[40] The deuteration provides contrast between the blocks, which is necessary for determining the number of microdomain layers using d-SIMS. Size exclusion chromatography before and after deuteration showed no change in molecular weights.[39]

To prevent charging at the interface with the substrate during d-SIMS experiments, all samples were prepared on a thick thermal oxide. A PlasmaTherm PECVD system was used to deposit 25 nm of silicon oxide onto a silicon wafer. The substrates were then cleaned using a piranha solution (3:1 H_2SO_4:H_2O_2 vol/vol) to remove any organic material. Films were prepared immediately after cleaning to ensure as little contamination as possible.

Thickness gradient samples were prepared at the National Institute for Standards and Technology Combinatorial Methods Center using a previously described method.[41] Block copolymer solutions of either 1.4 or 2 wt % were prepared, and 35 μL was placed under the 18 mm blade and accelerated at either 2 or 4 mm/s^2 from an initial velocity of 0 mm/s to a maximum velocity of 15 mm/s. The total distance traveled was 50 mm. Films were annealed under high vacuum (10^{-8} Torr) at 205 °C (above the ODT) for 12 h and then slowly cooled to either 125 or 165 °C where they were held for 3 days. They were then quenched to room temperature. The thickness at positions along the gradient was determined using a Filmetrics F20 UV−vis interferometer in reflectance mode with a spot size of 0.5 mm and an acquisition time of a few seconds. Measurements were taken at 5 mm increments in the x and y directions on the sample using a translation stage that rasters the film under the interferometer.

Tapping mode atomic force microscopy (AFM) measurements were made using a Digital Instruments Dimension 3000 atomic force microscope. Phase contrast images were collected over 2 μm × 2 μm regions to reveal the surface morphology. The hard PS blocks appear light in a dark matrix of soft PEB blocks. Images were collected using Applied Nanostructures long cantilevers (ACL). Tapping was sufficiently hard to tap through the soft surface layer of the ethylene−butylene block.

Dynamic secondary ion mass spectrometry (d-SIMS) was performed at UCSB using the primary O_2^+ ion beam of a Physical Electronics 6650 d-SIMS. The primary beam was operated at a beam voltage of 2 kV with a current of 40 nA. The beam was rastered over a 300 μm × 300 μm region of the sample, and a nonfocused, static 500 eV electron beam was used to provide charge compensation. Secondary ions were collected from a region within the area exposed to the primary ion beam, covering 120 μm × 120 μm. The sample was etched down to the silicon substrate, and the deuterium signal was tracked. Because of the selective deuteration, the maxima of the deuterium signal denote the layers of polystyrene domains. The sample stage was cooled with liquid nitrogen to cool the sample below the glass transition temperature of the ethylene−butylene matrix ($T_{g,EB}$ = −36 °C).[42] This is necessary because molecular fragments created by the primary beam are able to diffuse through a rubbery matrix.

Table 2. Number of Microdomain Layers, As Determined by d-SIMS, for Each Film Thickness of SEB Diblock Copolymer on Silicon Oxide Annealed at 165 °C[a]

thickness (nm)	no. of layers	structure
31	1	I (S)
38	1	H (S)
43	1	H (S)
48	1	F (S/C)
51	2	I (S/C)
54	2	I (S/C)
57	2	I (S/C)
60	2	I (S/C)
64	2	I (S/C)
71	3	H (C)
76	3	F (C)
84	4	I (C)
87	4	H (C)
96	4	H (C)

[a] The structure column indicates whether there is a flat film (F), islands (I), or holes (H) and also whether AFM shows spheres (S) or cylinders (C).

Grazing incidence small-angle X-ray scattering (GISAXS) measurements were performed at beamline 8-ID-E at the Advanced Photon Source of Argonne National Laboratory. The incident X-ray energy was 7.35 keV, with a wavelength of λ = 1.69 Å. The specular reflected intensity along the z-axis was blocked with a lead beam stop while the off-specular intensity in the $y-z$ plane outside the beam stop was recorded using a MAR-CCD 2D detector with a resolution of 79 μm/pixel. The sample-to-detector distance was calibrated with a silver behemate standard with a d-spacing of 58.376. The beam size was 100 μm in the horizontal (y) direction by 50 μm in the vertical (z) direction. Images were collected for 5−30 s depending on the strength of scattering and repeated five times. The data were stored as 2048 × 2048 tiff images. The incident angle was varied from α_i = 0.05°−0.21° in order to characterize both the surface and the entire film thickness. The critical angle for total external reflection of the polymer is 0.16°, and that of the silicon substrate is 0.23°. When the incident angle is below the critical angle of the polymer, approximately only the surface layer of domains of the film is being probed, but when the incident angle is between the critical angles of the polymer and the silicon substrate, the entire film thickness contributes to the scattered intensity. More details regarding the GISAXS analysis have been published elsewhere.[8]

Results

SEB Diblock Copolymer. Dynamic secondary ion mass spectrometry (d-SIMS) was used to determine the number of microdomain layers at each film thickness by tracking the deuterium signal, which is indicative of the polystyrene domains. Table 2 shows the number of microdomain layers as determined by d-SIMS as well as the morphology determined with AFM and GISAXS for each film thickness.

Figure 1 shows representative AFM phase images from SEB annealed at 165 °C for 3 days and quenched to room temperature. When the film is 31 nm thick, islands of spheres are surrounded by an SEB brush. Increasing the thickness to 38−43 nm creates a layer of hexagonally packed spheres with holes of SEB brush. A monolayer of mixed spheres and cylinders is seen when the film is 48 nm thick. The morphology remains mixed up to 64 nm, with the film forming islands to relieve the thickness frustration. At 71 nm, the morphology is mostly cylindrical, with spheres at the defects and at the edges of the holes in the film. Cylinders are present at 76 nm, with no islands or holes present. In thicker films, the dominant morphology remains cylindrical with relief structures of islands at 84 nm and holes from 87 to 96 nm. In all of these cases, the cylindrical regions are ≈2 nm thicker than the spherical ones, as determined by line scans on AFM height images.

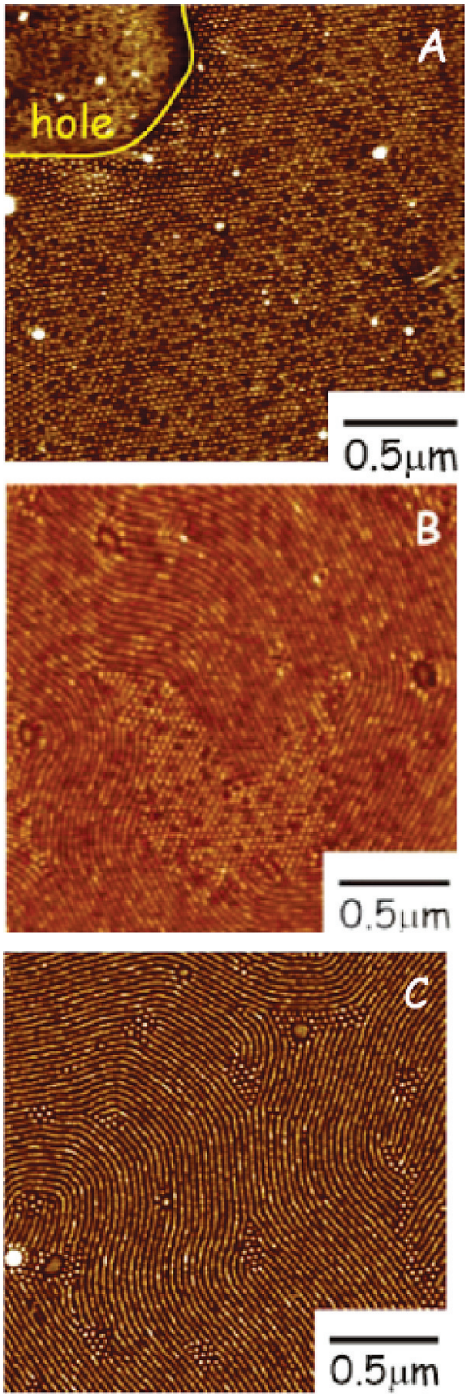

Figure 1. (A) AFM phase image of a 38 nm thick SEB film showing a layer of spheres that has holes with only SEB brush. (B) AFM phase image of a 60 nm thick SEB film showing a mixed morphology of cylinders and spheres. The spherical regions are 2 nm thinner than the cylindrical region, determined from AFM height images (not shown). At this film thickness, the film has one layers of cylinders plus islands of cylinders. (C) AFM phase image of a 71 nm thick SEB film showing a cylindrical morphology with spheres at the cores of defects. The film has three layers of microdomains with holes in the top layer (not shown) that go down to the second layer.

Because AFM samples only square micrometers, grazing incidence small-angle X-ray scattering (GISAXS) was performed to improve the statistics and confirm that the morphology seen in AFM is indeed the overall morphology.

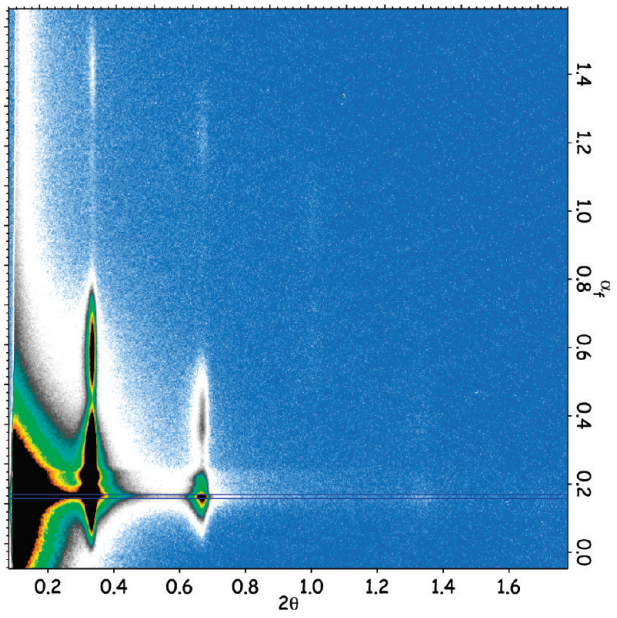

Figure 2. Two-dimensional scattering pattern at $\alpha_i = 0.17°$ showing higher order peaks in a 67 nm thick SEB film annealed at 165 °C for 3 days and quenched to room temperature. The blue horizontal lines indicate the positions between which the line scan was extracted.

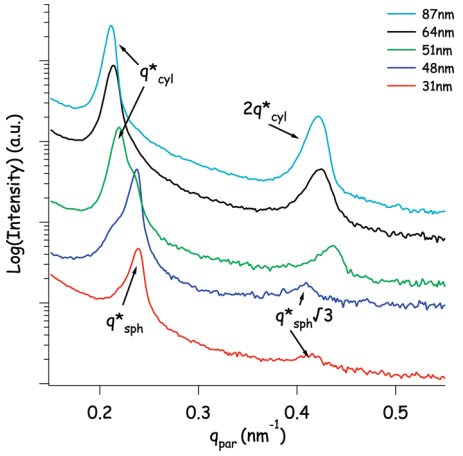

Figure 3. Line profiles of in-plane scattering for SEB diblock on silicon oxide annealed 3 days at 165 °C and quenched to room temperature. The line profiles were extracted from scattering patterns at $\alpha_i = 0.17°$. The ratio of the peaks changes from 1:$\sqrt{3}$ for hexagonally packed spheres to 1:2 for cylinders oriented parallel to the substrate.

GISAXS measurements cover square millimeters of the sample and therefore have significantly better statistics than AFM measurements in addition to being able to provide more accurate lattice parameters. Analysis of the scattering as a function of the incident angle has shown that the morphology is constant throughout the depth of the film, so in this paper the only data shown are for $\alpha_i = 0.17°$, which provides data for the entire film thickness.[39] The Supporting Information shows the in-plane scattering for several values of α, with values both above and below the critical angle of the polymer.

Figure 2 shows the relevant portion of the 2d scattering pattern for a 67 nm thick sample. In-plane scattering line scans were extracted from the 2d scattering patterns to determine the microdomain morphology. Figure 3 shows the in-plane line scans, along 2θ, from several film thicknesses. In the films that show a spherical morphology by

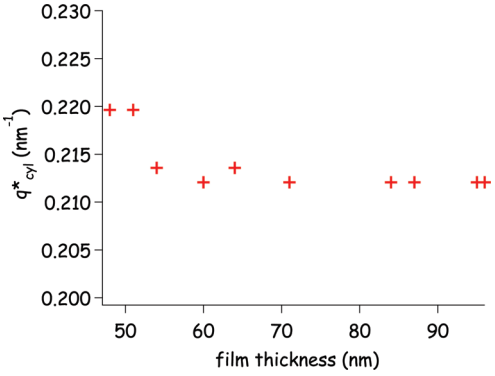

Figure 4. Position of q^*_{cyl} peak as a function of film thickness for SEB diblock on silicon oxide annealed at 165 °C. The q^*_{cyl} value decreases when the film is predominantly cylinders, indicating that the intercylinder spacing increases with film thickness.

Table 3. Number of Microdomain Layers, As Determined by d-SIMS, for Each Film Thickness of SEB Diblock Copolymer on Silicon Oxide Annealed at 125 °C[a]

thickness (nm)	no. of layers	structure
32	1	I (S/C)
35	1	H (S/C)
41	1	H (S/C)
43	1	F (S)
45	1	F (S/C)
50	1	F (S/C)
52	2	F (C)
53	2	I (C)
61	2	I (C)
65	2	H (C)
67	2	F (C)
70	3	I (C)
73	3	H (C)
76	3	H (C)
80	3	H (C)
82	3	H (C)

[a] The structure column indicates whether there is a flat film (F), islands (I), or holes (H) and also whether AFM shows spheres (S) or cylinders (C).

AFM, the peak positions are in a q/q^* ratio of 1:$\sqrt{3}$:2, which is characteristic of hexagonal packing. The nearest-neighbor spacing for the hexagonal spheres is $a = 30$ nm and does not change as the film thickness increases. Films that show cylinders in the AFM show peak positions in a q/q^* ratio of 1:2:3, corresponding to a layer of cylinders oriented parallel to the substrate. At thicknesses where the morphology is a mixed monolayer of spheres and cylinders, there are peaks corresponding to both q/q^* ratios. The peak position of the q^*_{cyl} moves to lower values of q when the film changes from a mixture of spheres and cylinders to predominantly cylinders. Figure 4 shows how the value of q^*_{cyl} changes with increasing film thickness. Once the film consists of three layers of cylinders, the value of q^*_{cyl} remains nearly constant as the film thickness increases. The cylinder spacing ranges from 28.6 to 29.6 nm over this thickness range. These numbers are in qualitative agreement with the values obtained from AFM data, which is less accurate due to drift and distortion of the AFM.

Films with the same thickness range were annealed at 125 °C, below the bulk OOT, and characterized in the same method. Table 3 shows the number of microdomain layers at each film thickness, as determined by d-SIMS. One of the most noticeable differences between samples annealed at 125 and 165 °C is that the islands formed in films annealed at 125 °C have cylinders in the center of the island, surrounded

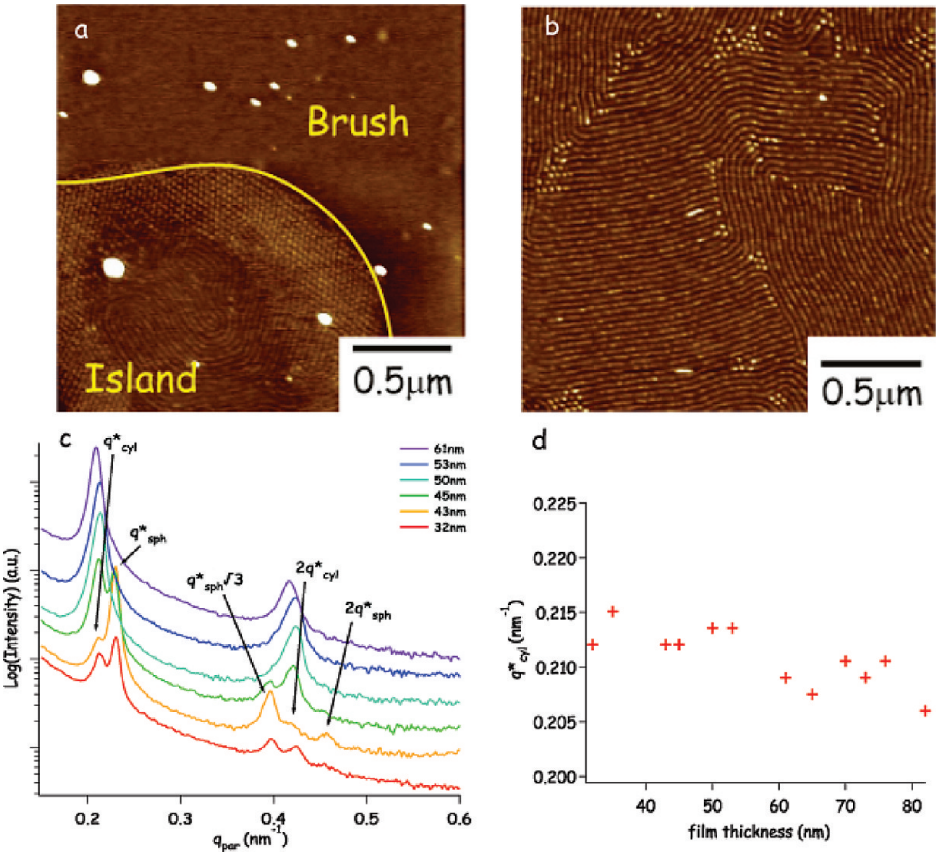

Figure 5. Results from SEB films annealed at 125 °C. (a) AFM image of a 32 nm thick film showing an island with cylinders in the center, surrounded by spheres. (b) AFM image of a 67 nm thick film showing the dominant cylindrical morphology. (c) In-plane GISAXS profiles showing the change in morphology as a function of increasing film thickness. (d) Position of the q^*_{cyl} peak as a function of increasing film thickness.

Table 4. Number of Polystyrene Microdomain Layers for Each Film Thickness That Was Annealed at 125 °C, As Determined with d-SIMS[a]

thickness (nm)	no. of layers	structure
30	1	I
32	1	H
37	1	F
45	1	F
48	1	F
54	1	I
56	2	H
57	2	I
61	2	I
62	2	I
69	3	H
75	3	F
82	4	H
89	4	H
94	4	I
96	4	I

[a] The presence of islands or holes in the film is indicated in the right column.

by spheres, instead of only spheres on the islands. Figure 5 shows a summary of the results when the films are annealed below the bulk OOT. The results are in qualitative agreement with those for films annealed above the bulk OOT.

SEBS Triblock Copolymer. Table 4 shows the number of microdomain layers for each film thickness, determined by d-SIMS, of SEBS triblock copolymer on silicon oxide annealed at 125 °C. Atomic force microscopy (AFM) was used to examine the surface morphology at each film thickness. In all cases the morphology was spherical. Figure 6 shows an AFM phase image of a 37 nm thick film annealed at 125 °C for 3 days and quenched to room temperature. This is indicative of the AFM data over the entire thickness range. Islands or holes form when the film thickness does not match that for an integral number of spherical layers in order to lower the overall free energy.

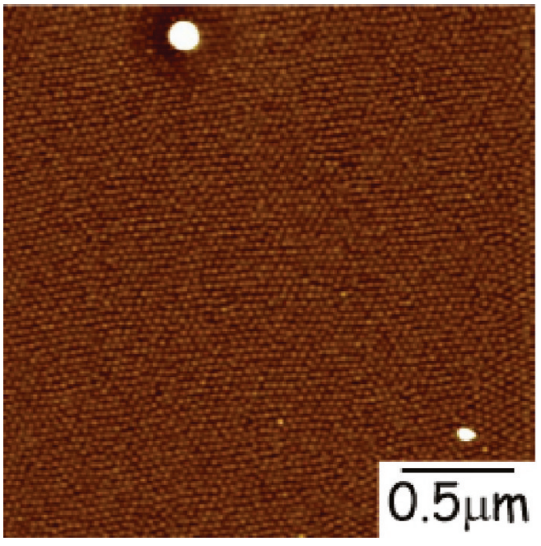

Figure 6. AFM phase image showing the spherical morphology of a 37 nm thick SEBS film on silicon oxide annealed at 125 °C for 3 days and quenched to room temperature.

GISAXS was also used to study the packing of the spherical domains because AFM does not have sufficient accuracy to distinguish between hexagonal or other packing

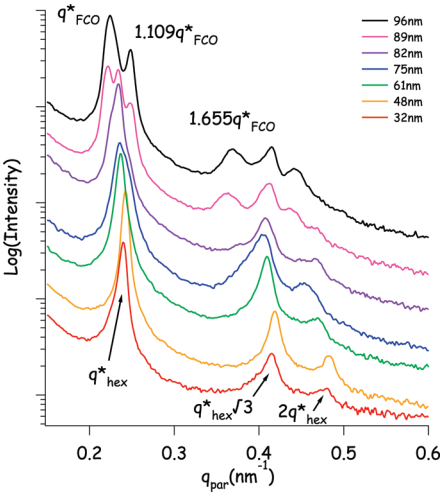

Figure 7. Line profiles showing the in-plane scattering from SEBS triblock on silicon oxide annealed at 125 °C showing the transition from hexagonal to face-centered orthorhombic packing of the spherical microdomains.

of spheres or to accurately determine the lattice parameters. In-plane scattering profiles extracted from the 2-dimensional scattering patterns are shown in Figure 7. The q/q^* ratio of the peak positions changes from $1:\sqrt{3}:2$ for the hexagonal lattice to approximately 1:1.109:1.655 for a face-centered orthorhombic (FCO) lattice as the film thickness increases. In films up through 48 nm, the system is hexagonal with a nearest-neighbor spacing of $a = 30.3$ nm. When the films are 61 and 75 nm thick, the packing is still hexagonal, but with a slightly larger nearest-neighbor spacing of $a = 30.7$ nm. There is a stretching of the lattice as the film thickness increases but the packing remains hexagonal. When the film is 75 nm thick, the nearest-neighbor spacing is $a = 30.9$ nm, which corresponds to a stretching of just over 1%. At 82 nm, there appears to be a coexistence of the hexagonal and FCO phases, with the transition to FCO complete at 96 nm.

The results for thin films annealed above the bulk OOT, at 165 °C, are nearly the same as the results for films annealed at 125 °C and are summarized in Figures 8 and 9. The GISAXS peaks are more narrow at 165 °C than at 125 °C due to the smaller grain size and high dislocation density of the sphere layers at 125 °C, as can be seen in the AFM micrograph of Figure 6. The spherical morphology transitions from hexagonal to FCO packing at four layers of spheres.

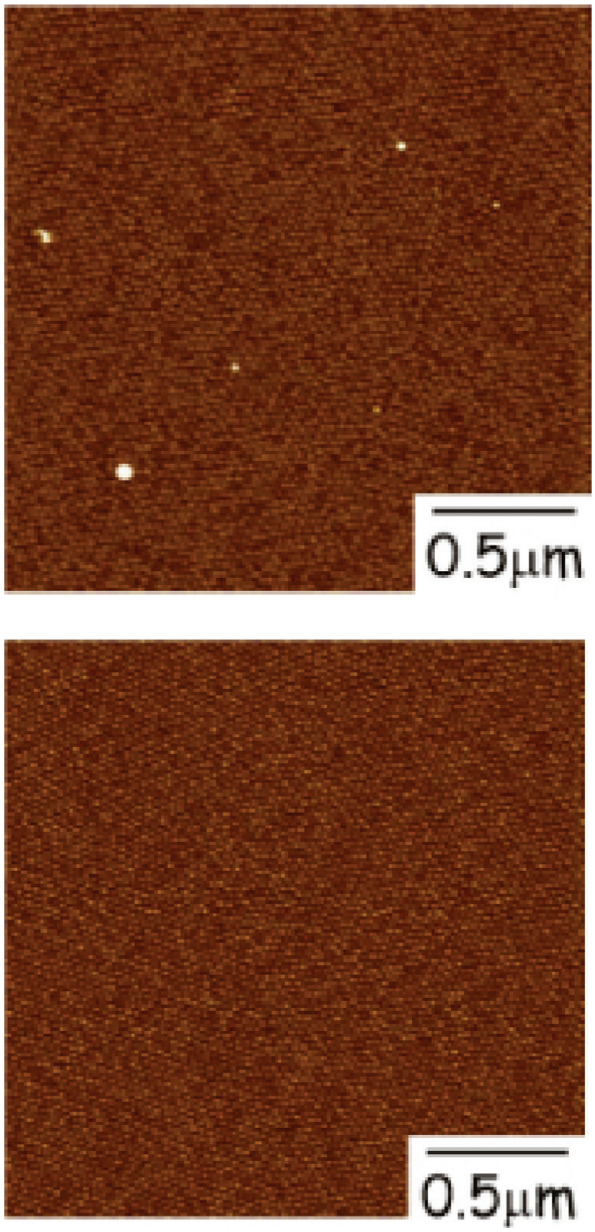

Figure 8. Top: AFM phase image of a 38 nm thick SEBS film annealed at 165 °C. Bottom: AFM phase image of an 82 nm thick SEBS film annealed at 165 °C.

Discussion

At an annealing temperature of 165 °C that is well above the bulk OOT, the triblock copolymer SEBS thin film morphology is spherical. Surprisingly, however, at 125 °C, well below the OOT of 140 °C, where the bulk morphology is cylindrical, the thin film morphology is also spherical for all film thicknesses investigated. We first try to understand the possible reasons for this apparent suppression of the OOT in these triblock copolymer films in terms of the packing frustration in the Wigner−Seitz (W−S) cells of the spherical and cylindrical morphology.

Figure 10 shows schematic drawings of the free energy per chain for a monolayer and the bulk for the spherical and cylindrical phases. The free energy per chain for the spheres is plotted as a function of the order parameter, η, which is defined as $\eta = a_1/a_2$, where a_2 is the nearest-neighbor distance and a_1 is the next-nearest-neighbor distance in the plane of the film. The free energy per chain of the cylinders is plotted as a function of the nearest-neighbor distance. In the case of the spheres, there is also a local minimum in the bulk free energy per chain for the hexagonal phase ($\eta = 1$), but there is a global minimum that corresponds to the BCC phase ($\eta = 1.154$) because the BCC structure requires less nonuniform stretching of the corona chains to fill its interstices in the bulk than does the hexagonal close-packed structure.[43−45] At the OOT, the free energies of the BCC and the cylinder bulk morphologies are the same, but for both morphologies, the free energies per chain of the monolayers are higher than those of the bulk because chains are stretched more nonuniformly in Wigner−Seitz (W−S) cells at the surface than in the bulk in order to fill the interstices and provide a constant polymer density. The optimum cell shape for cylinders for example is a circular unit cell, which would eliminate any nonuniform chain stretching. However, circular unit cells cannot pack to fill space. Any deviation from this circular unit cell results in additional chain stretching ("packing frustration").[45] The Wigner−Seitz cell for the cylinder monolayer is a square cross-section rod while that for the hexagonal array of spheres in the sphere monolayer is a hexagonal prism, as seen in Figure 11.

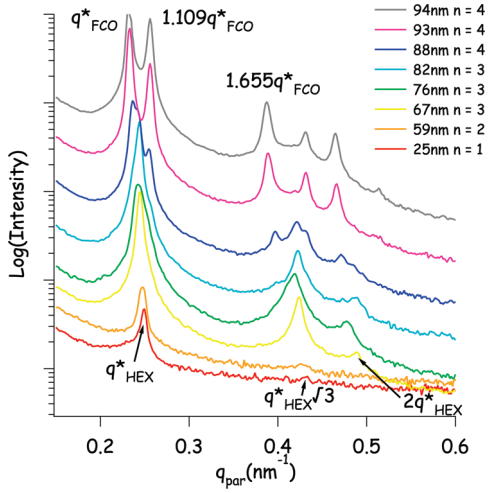

Figure 9. GISAXS in-plane scattering profiles as a function of film thickness showing the transition from hexagonal to FCO packing at an annealing temperature of 165 °C.

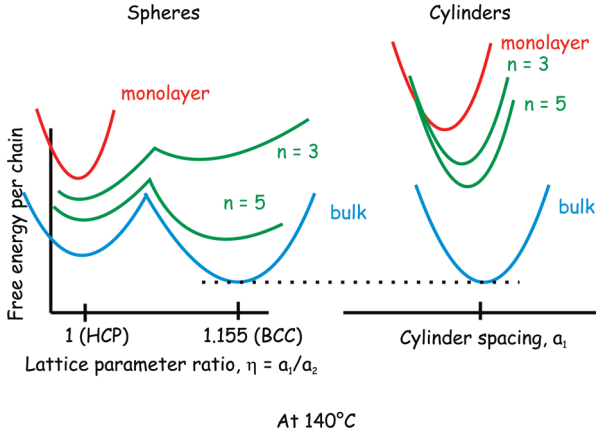

Figure 10. Schematic diagram of the free energy per chain for the spherical and cylindrical phases at the OOT. The bulk free energies per chain of the two phases are equal, but the difference in free energies per chain of the spherical and cylindrical monolayers is what dictates the thin film behavior. This diagram does not contain any contribution to the free energy per chain due to chain ends near the surface of the film.

Olmstead and Milner[46,47] estimate the ratio of the free energy per chain for cylinders in a square Wigner−Seitz cell to that for cylinders in a hexagonal one to be 1.063 and compared that to the ratio they found (1.005) between these quantities for an FCC versus a BCC W−S cell for spheres. As expected, the "roundest" Wigner−Seitz cells have the least packing frustration and the lowest free energy per chain. This result suggests that the increase in the free energy, Δf, per chain for the cylinder monolayer relative to a cylinder layer in the bulk is likely to be larger than the increase Δf of a hexagonal monolayer of spheres over a (110) BCC layer of spheres in the bulk. The hexagonal W−S cell of the sphere monolayer has on average a significantly more rounded form than the square W−S cell of the cylinder monolayer and thus is expected to have a smaller free energy increase over the bulk due to packing frustration. Note that for bilayers, trilayers, and multilayers the W−S cell for the top half (and bottom half) of the layers at the surfaces is identical in shape to that of the monolayer, as first pointed out by Knoll et al. and as shown schematically in Figure 12; therefore, the packing frustration penalty for cylindrical surface layers over sphere surface layers will persist, but its contribution to the free energy per block copolymer chain will decrease approximately as $1/n$ where n is the number of cylinder or sphere layers as estimated by Knoll et al.[48]

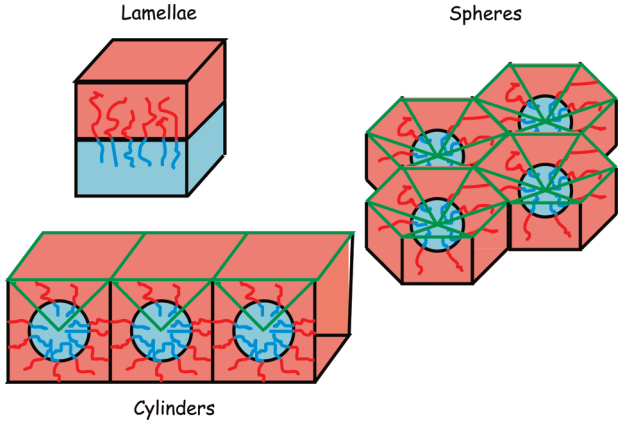

Figure 11. Schematic showing the Wigner−Seitz cells of a monolayer of lamella, of cylinders, and of spheres as well as the differing fractions of diblock copolymer chains that can have their chain ends at the surface for each morphology. The free energy decrease due to the entropy of these chain ends is largest for the lamellar morphology and smallest in the spherical morphology.

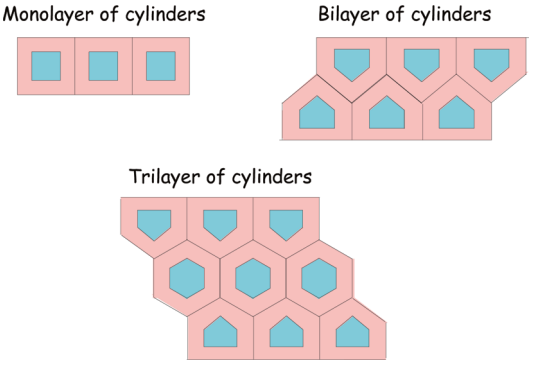

Figure 12. Schematic illustrating the Wigner−Seitz cells required for a monolayer, bilayer, and trilayer of cylinders, leading to extra packing frustration if block copolymer domains near the surface (after Knoll et al.[48]).

Eventually for large n, this will mean that the free energy per chain, and the OOT of the film, must approach those of the bulk. Evidently, this does not occur for $n < 5$ since we observe the spherical morphology even at 125 °C for such films of the SEBS.

The transition observed in the spherical morphology of the SEBS from hexagonal to face-centered orthorhombic (FCO) as n increases is expected based on the results of both self-consistent-field theory simulations and experiments for block copolymers with aspherical morphology at all temperature (no OOT).[8,44] As illustrated schematically in Figure 10, as the number of layers increases, a second minimum forms at a value of η intermediate between 1 and 1.1545, corresponding to a FCO structure. This minimum results from a competition between the free energy versus η of the preferred morphology for the surface layers (hexagonal) and that of the preferred morphology ((110) BCC) for the inner layers of the film. Nevertheless, it is clear that the difference in free energy between spheres and cylinders is very small so that small changes in the free energy of the surface layers, the layers with maximum packing frustration, may be sufficient to cause cylinders to be more stable than spheres. We consider next what subtle free energy changes there might be that would tip the balance toward cylinders for the diblock copolymer SEB.

The free energy diagram shown schematically in Figure 10 is the reason behind the OOT transition at a fixed number of layers. Clearly, if spheres are not observed at these thicknesses for the diblock copolymer, some factor other than those considered so far for the triblock copolymer must decrease the free energy per

chain of the diblock SEB cylinders to below that for the spheres. The deviation of the SEB diblock copolymer thin film morphology from that of the SEBS triblock copolymer can be qualitatively understood by considering the difference in the chain topology between the diblock and triblock that must occur in order to populate the surface with the lower surface energy PEB midblock. Light tapping in AFM shows no structure in the phase image, indicating that there is a thin PEB block layer covering the polystyrene domains, and this conclusion is verified by the dynamic SIMS experiments. The segregation of the PEB block to the surface is due to the lower surface energy of the EB midblock (γ_{PEB} = 17.6 mJ/m^2) compared to the end blocks (γ_{PS} = 40 mJ/m^2).[49,50] In the case of the diblock copolymer, the matrix PEB end block will organize such that the ends of these chains are near the free surface, but in addition to the packing frustration already discussed, this organization may bias the free energy in favor of cylinders. In the case of the triblock copolymer surface layer no chain ends can be present near the surface. All the midblocks must either loop back to the same domain or bridge to an adjacent domain.

The effects of forced looping back of midblock chains on the surface energy have been previously discussed in terms of a free energy penalty for looping.[49,51−53] A very recent theoretical paper by Matsen,[54] however, casts this problem in a very different light. He shows for lamellar block copolymers that the chain ends of diblock copolymer near the surface have an extra entropy that leads to a decrease in surface tension $-\Delta\gamma$ whose value is given by

$$-\Delta\gamma = \frac{1.51 w_s k_B T \rho_0}{N} \quad (1)$$

where ρ_0 is the block copolymer segment density, N is the degree of polymerization of the block copolymer, and w_s is the thickness of the region at the surface over which the polymer density falls to zero. In his theory it is this extra entropy of the chain ends at the surface, not an entropy penalty for looping, that is important. In applying Matsen's ideas to our problem, we note that it is the free energy per chain in the cylinder or sphere structure that determines which structure is stable near the OOT. Since ρ_0/N is a polymer number density, the contribution of the entropy of chain ends near the surface to the free energy per chain f_e of the lamellar diblock copolymer film is

$$f_e = \frac{-1.52 w_s k_B T}{t} \quad (2)$$

where t is the thickness of the block copolymer layer. In the case of a lamellar AB diblock copolymer in an orientation parallel to the surface, all the chains that emerge from the AB interface have their ends near the surface. In the cylindrical morphology, however, only about one-half the chains that emerge from the top half of the cylinder can have their ends near the surface, as shown schematically in Figure 11. If all ends of the chains from the top half of the cylinder were to be positioned near the surface, the packing frustration would be extreme. Therefore, the contribution of the entropy of chain ends near the surface to the free energy per chain $f_{e,cylinders}$ of the cylindrical diblock copolymer should be

$$f_{e,\,cylinders} = \frac{-0.72 w_s k_B T}{t} \quad (3)$$

In the sphere morphology the fraction of chains emerging from the top half of a sphere that can have their ends near the surface is even less; only those within a hexagonal base pyramid with its apex in the sphere center can locate their ends near the surface. From the geometry only a fraction $\approx 1/3$ of the chains that emerge from the top half of the sphere have their ends near the surface, as shown schematically in Figure 11. Thus, the contribution of the entropy of chain ends near the surface to the free energy per chain $f_{e,spheres}$ of the spherical diblock copolymer should be

$$f_{e,\,spheres} = -\frac{0.51 w_s k_B T}{t} \quad (4)$$

Thus, the free energy per chain of a layer of diblock block copolymer cylinders will be lower than that of diblock copolymer spheres by $0.21 w_s k_B T/t$. This contribution is apparently decisive in favoring the SEB cylinders over SEB spheres at temperatures between 125 and 165 °C. However, in the triblock SEBS copolymer this entropic contribution favoring the cylinders is missing, and evidently that increase in the free energy per chain of the cylinder phase relative to the spheres is enough to stabilize the spheres over the range of temperature between 125 and 165 °C.

As the number of layers of SEB diblock copolymer cylinders increases, the nearest-neighbor distance increases but at a decreasing rate with film thickness, and thus n, as shown by Knoll et al.[48] The bulk cylinder−cylinder spacing for this diblock copolymer is 32 nm at this temperature, which is larger than any of the cylinder−cylinder spacings seen in our thin films. Our results are in qualitative agreement with the experiments of Knoll et al., who systematically measured the cylinder−cylinder spacing change as a function of increasing film thickness using AFM and found that as the number of layers increases, the cylinder−cylinder spacing approaches the bulk value.[48] They used the strong-stretching theory of Olmsted and Milner to estimate the equilibrium W−S cell widths for each film thickness (see Figure 12).[46,47] Their estimates show that the width of the square unit cell of the monolayer is 6% less than that of the hexagonal unit cell of the bulk cylinders. Our results for the changes in the cylinder spacing are in qualitative agreement with both their experiments and their estimates, bearing in mind that our GISAXS results at thicknesses that have islands or holes are an area-weighted average whereas they could measure local values of cylinder spacing with an AFM.

Conclusions

Thin films of SEBS triblock copolymer have a spherical morphology even at a temperature significantly below the bulk order−order transition where a cylinder morphology would be seen in the bulk. The larger packing frustration of block copolymer chains in the surface layers of the cylindrical morphology apparently increases its free energy relative to that of the spherical morphology. Thin films of the complementary SEB diblock copolymer show almost the opposite behavior. In these diblock films cylinders are formed even well above the OOT of the bulk, except under the following conditions: when the film thickness is below the ideal thickness of a layer of cylinders or when the thickness requires the formation of islands or holes. In the latter case the spherical morphology appears at the edges of islands and holes. We hypothesize that the larger free energy of the diblock copolymer chains in cylinders due to their larger packing frustration in the surface Wigner−Seitz cells is more than offset by a larger entropy due to their chain ends at the surface relative to these quantities for the spherical morphology. Detailed self-consistent field or other simulations that can detect the subtle changes in free energy due to the surfaces are needed to test this hypothesis rigorously.

Acknowledgment. Primary funding was provided by the National Science Foundation DMR Polymers Program under Award DMR-07-04539 and by the NSF Graduate Research Fellowship with secondary funding provided by the ONR under

Grant N00014-02-1-0170. The Advanced Photon Source at Argonne National Laboratory is funded by the DOE Division of Basic Energy Sciences by Grant W-31-109-ENG-38. Some of the work presented was conducted at the NIST Combinatorial Methods Center. Terence Choy (now at UC Berkeley) separated the diblock and triblock from the blend and was funded by the NSF-REU program. This work made use of central facilities at the MRL at UCSB, which is funded by the MRSEC program of the NSF under Grant DMR05-20415, and from use of the nanofabrication facilities, which is supported by the NSF-NNIN under Award 44771-7475. Dale Handlin from Kraton provided the commercial polymer blend. We acknowledge many helpful discussions with Mark Matsen (Reading) as well as with Glenn Fredrickson (UCSB) on differences between diblock copolymers and triblock copolymers. Gila Stein (Houston), Vindhya Mishra, and Kristin Schmidt (UCSB) are thanked for useful discussions on the GISAXS analysis.

Supporting Information Available: In-plane scattering profiles for various incident X-ray angles from a 76 nm thick SEB diblock copolymer thin film. This material is available free of charge via the Internet at http://pubs.acs.org.

References and Notes

(1) Bates, F. S.; Fredrickson, G. H. *Annu. Rev. Phys. Chem.* **1990**, *41*, 525–557.
(2) Bates, F. S.; Fredrickson, G. H. *Phys. Today* **1999**, *52*, 1999.
(3) Segalman, R. A.; Yokoyama, H.; Kramer, E. J. *Adv. Mater.* **2001**, *13*, 1152–1155.
(4) Kim, S. O.; Solak, H. H.; Stoykovich, M. P.; Ferrier, N. J.; de Pablo, J. J.; Nealey, P. F. *Nature* **2003**, *424*, 411–414.
(5) Harrison, C.; Angelescu, D. E.; Trawick, M.; Cheng, Z. D.; Huse, D. A.; Chaikin, P. M.; Vega, D. A.; Sebastian, J. M.; Register, R. A.; Adamson, D. H. *Europhys. Lett.* **2004**, *67*, 800–806.
(6) Hammond, M. R.; Cochran, E.; Fredrickson, G. H.; Kramer, E. J. *Macromolecules* **2005**, *38*, 6575–6585.
(7) Stoykovich, M. P.; Müller, M.; Kim, S. O.; Solak, H. H.; Edwards, E.; de Pablo, J. J.; Nealey, P. F. *Science* **2005**, *308*, 1442–1446.
(8) Stein, G. E.; Kramer, E. J.; Li, X. F.; Wang, J. *Macromolecules* **2007**, *40*, 2453–2460.
(9) Ruiz, R.; Ruiz, N.; Zhang, Y.; Sandstrom, R. L.; Black, C. T. *Adv. Mater.* **2007**, *19*, 2157.
(10) Bosworth, J. K.; Andre, X.; Schwartz, E. L.; Ruiz, R.; Black, C. T.; Ober, C. K. *J. Photopolym. Sci. Technol.* **2007**, *20*, 519–522.
(11) Stoykovich, M. P.; Kang, H.; Daoulas, K. C.; Liu, G.; Liu, C.; de Pablo, J. J.; Müller, M.; Nealey, P. F. *ACS Nano* **2007**, *1*, 168–175.
(12) Sakurai, S.; Kawada, H.; Hashimoto, T.; Fetters, L. J. *Macromolecules* **1993**, *26*, 5796–5802.
(13) Koppi, K. A.; Tirrell, M. V.; Bates, F. S.; Almdal, K.; Mortensen, K. *J. Rheol.* **1994**, *114*, 999–1027.
(14) Modi, M. A.; Krishnamoorti, R.; Tse, M. F.; Wang, H.-C. *Macromolecules* **1999**, *32*, 4088–4097.
(15) Mani, S.; Weiss, R. A.; Cantino, M. E.; Khairallah, L. H.; Hahn, S. F.; Williams, C. E. *Eur. Polym. J.* **2000**, *36*, 215–219.
(16) Kimishima, K.; Koga, T.; Hashimoto, T. *Macromolecules* **2000**, *33*, 968–977.
(17) Krishnamoorti, R.; Modi, M. A.; Tse, M. F.; Wang, H.-C. *Macromolecules* **2000**, *33*, 3810–3817.
(18) Matsen, M. W. *J. Chem. Phys.* **2001**, *114*, 8165–8173.
(19) Nonomura, M.; Yamada, K.; Ohta, T. *J. Phys.: Condens. Matter* **2003**, *15*, L423–L430.
(20) Yamada, K.; Nonomura, M.; Ohta, T. *Macromolecules* **2004**, *37*, 5762–5777.
(21) Lai, C. J.; Loo, Y. L.; Register, R. A. *Macromolecules* **2005**, *38*, 7098–7104.
(22) Sota, N.; Sakamoto, N.; Saijo, K.; Hashimoto, T. *Polymer* **2006**, *47*, 3636–3649.
(23) Honda, T.; Kawakatsu, T. *Macromolecules* **2006**, *39*, 2340–2349.
(24) Schmidt, K.; Schoberth, H. G.; Schubert, F.; Hänsel, H.; Fischer, F.; Weiss, T. M.; Sevink, G. J. A.; Zvelindovsky, A. V.; Böker, A.; Krausch, G. *Soft Matter* **2007**, *3*, 448–453.
(25) Liu, Y.; Li, M.; Bansil, R.; Steinhart, M. *Macromolecules* **2007**, *40*, 9482–9490.
(26) Wang, C.-Y.; Lodge, T. P. *Macromolecules* **2002**, *35*, 6997–7006.
(27) Hanley, K. J.; Lodge, T. P. *J. Polym. Sci., Part B: Polym. Phys.* **1998**, *36*, 3101–3113.
(28) Xu, T.; Zvelindovsky, A. V.; Sevink, G. J. A.; Gang, O.; Ocko, B.; Zhu, Y.; Gido, S. P.; Russell, T. P. *Macromolecules* **2004**, *37*, 6980–6984.
(29) Xu, T.; Zvelindovsky, A. V.; Sevink, G. J. A.; Lyakhova, K. S.; Jinnai, H.; Russell, T. P. *Macromolecules* **2005**, *38*, 10788–10798.
(30) Shin, C.; Ryu, D. Y.; Huh, J.; Kim, J. H.; Kim, K.-W. *Macromolecules* **2009**, *42*, 2157–2160.
(31) Anastasiadis, S. H.; Russell, T. P.; Satija, S. K.; Majkrzak, C. F. *Phys. Rev. Lett.* **1989**, *62*, 1852–1855.
(32) Karim, A.; Singh, N.; Sikka, M.; Bates, F. S.; Dozier, W. D.; Felcher, G. P. *J. Chem. Phys.* **1994**, *100*, 1620–1629.
(33) Knoll, A.; Horvat, A.; Lyakhova, K. S.; Krausch, G.; Sevink, G. J. A.; Zvelindovsky, A. V.; Magerle, R. *Phys. Rev. Lett.* **2002**, *89*.
(34) Ludwigs, S.; Krausch, G.; Magerle, R.; Zvelindovsky, A. V.; Sevink, G. J. A. *Macromolecules* **2005**, *38*, 1859–1867.
(35) Ludwigs, S.; Schmidt, K.; Stafford, C. M.; Amis, E. J.; Fasolka, M. J.; Karim, A.; Magerle, R.; Krausch, G. *Macromolecules* **2005**, *38*, 1850–1858.
(36) Knoll, A.; Lyakhova, K. S.; Horvat, A.; Krausch, G.; Sevink, G. J. A.; Zvelindovsky, A. V.; Magerle, R. *Nat. Mater.* **2004**, *3*, 886–890.
(37) Knoll, A.; Magerle, R.; Krausch, G. *J. Chem. Phys.* **2004**, *120*, 1105–1116.
(38) Silva, A. S.; Mitchell, C. A.; Tse, M. F.; Wang, H.-C.; Krishnamoorti, R. *J. Chem. Phys.* **2001**, *115*, 7166–7174.
(39) Sohn, K. E. Ph.D. Thesis, University of California, Santa Barbara, **2008**.
(40) Willenberg, B. *Makromol. Chem., Macromol. Chem. Phys.* **1976**, *177*, 3625–3628.
(41) Stafford, C. M.; Roskov, K. E.; Epps, T. H.; Fasolka, M. J. *Rev. Sci. Instrum.* **2006**, *77*, 023908.
(42) Chang, Y.-W.; Shin, J. -Y.; Ryu, S. H. *Polym. Int.* **2004**, *53*, 1047–1051.
(43) Thomas, E. L.; Kinning, D. J.; Alward, D. B.; Henkee, C. S. *Macromolecules* **1987**, *20*, 2934–2939.
(44) Stein, G. E.; Kramer, E. J.; Li, X.; Wang, J. *Phys. Rev. Lett.* **2007**, *98*.
(45) Matsen, M. W. *J. Phys.: Condens. Matter* **2002**, *14*, R21–R47.
(46) Olmsted, P. D.; Milner, S. T. *Phys. Rev. Lett.* **1995**, *74*, 829.
(47) Olmsted, P. D.; Milner, S. T. *Macromolecules* **1998**, *31*, 4011–4022.
(48) Knoll, A.; Tsarkova, L.; Krausch, G. *Nano Lett.* **2007**, *7*, 843–846.
(49) Khanna, V.; Cochran, E. W.; Hexemer, A.; Stein, G. E.; Fredrickson, G. H.; Kramer, E. J.; Li, X.; Wang, J.; Hahn, S. F. *Macromolecules* **2006**, *39*, 9346–9356.
(50) Ansari, I. A.; Clarke, N.; Hutchings, L. R.; Pillay-Narrainen, A.; Terry, A. E.; Thompson, R. L.; Webster, J. R. P. *Langmuir* **2007**, *23*, 4405–4413.
(51) Ten Brinke, G.; Hadziioannou, G. *Macromolecules* **1987**, *20*, 486–489.
(52) De Jeu, W. H.; Lambooy, P.; Hamley, I. W.; Vaknin, D.; Pedersen, J. S.; Kjaer, K.; Seyger, R.; Vanhutten, P.; Hadziioannou, G. *J. Phys. II* **1993**, *3*, 139–146.
(53) Balsara, N. P.; Tirrell, M. V.; Lodge, T. P. *Macromolecules* **1991**, *24*, 1975–1986.
(54) Matsen, M. W. *Macromolecules* **2010**, *43* 1671−1674.